Composites: Part A 161 (2022) 107072

Contents lists available at ScienceDirect

Composites Part A

journal homepage: www.elsevier.com/locate/compositesa

A damage constitutive model for the nonlinear mechanical behavior of C/SiC composites during mechanical cyclical loading/unloading

Z.B. Niu [a,b], S.A. Chen [a,*], Y. Li [b,*], P. Xiao [b], Z.M. Yang [c], Y.G. Tong [d], R.S.M. Almeida [e]

[a] Science and Technology on Advanced Ceramic Fibers and Composites Laboratory, National University of Defense Technology, Changsha 410073, China
[b] National Key Laboratory of Science and Technology on High-strength Structural Materials, Central South University, Changsha 410083, China
[c] Institute of Mechanics, Chinese Academy of Sciences, Beijing 100190, China
[d] College of Automobile and Mechanical Engineering, Changsha University of Science and Technology, Changsha, China
[e] Advanced Ceramics, University of Bremen, Bremen 28359, Germany

ARTICLE INFO

Keywords:
C/SiC composite
Nonlinear mechanical behavior
Damage mechanisms
Damage constitutive model

ABSTRACT

In this study, the nonlinear mechanical behavior and corresponding damage mechanisms of C/SiC composites during cyclic loading/unloading tensile tests were studied. Besides, based on the composite microstructure and damage mechanisms, the damage evolution model and single fiber unit model are proposed to explain the stiffness degradation, inelastic deformation accumulation, and elastic deformation. According to the stiffness degradation law, the damage evolution model based on Weibull failure probability is established, which can fit damage-strain curves well. Additionally, the single fiber unit model considering the microscopic mechanisms of matrix cracking, interfacial debonding, and sliding is established. In the model, the stress distributions before and after loading and unloading are analyzed to obtain the elastic strain and inelastic strain formulas of the composite that can perfectly fit the experimental results ($R^2 > 99.9\%$). Because the model reflects the deformation mechanisms of the composites in a much more simplified way, the deformation and damage law of the composite can be well predicted with basic macroscopic parameters such as the composition of the composite, the elastic modulus of the fiber, matrix, and composite, the strength of the matrix and the residual thermal stress of the matrix.

1. Introduction

Carbon fiber reinforced silicon carbide (C/SiC) composites have low density, favorable high-temperature mechanical properties, high resistance to corrosion and oxidation, and excellent thermal shock resistance [1–3]. As a new type of high-temperature structural material that can survive environmental temperatures of up to 1650 °C, it has become an indispensable material for aerospace components such as aircraft brakes, thermal protection systems for space shuttles, and nozzle-throats for aerospace engines, etc.

C/SiC composites overcome the brittleness of monolithic SiC ceramics due to the fiber reinforcement and controlled microstructure. Specifically, the introduction of carbon fibers makes the fracture process show characteristics of pseudo-plasticity by various mechanisms such as fiber debonding, pull out and crack bridging, which greatly improves the damage tolerance and reliability of these materials [4]. However, when the load exceeds the elastic limit that is far lower than the fracture limit, irreversible damage occurs in the form of matrix cracking, interfacial debonding, interfacial slip, single fiber, and fiber bundle fracture causing a decrease in mechanical properties [5]. As this irreversible damage accumulates to the damage tolerance of the material, fatigue fracture occurs.

Due to the generally low elastic limit of C/SiC composites (20 MPa), C/SiC composites inevitably suffer different degrees of damage under working conditions. Therefore, a damage constitutive model that can reflect its nonlinear behavior and damage mechanics is necessary for reliability of design and application of C/SiC composites [6–7]. Up to now, the damage behaviors and mechanisms of ceramic matrix composites (CMCs) have been widely studied via different methods such as in-situ observation, acoustic emission, and X-ray CT imaging [8–10]. According to the damage behaviors and mechanisms, a variety of constitutive models have been proposed, such as continuum damage model (CDM) based on continuum damage mechanics and thermodynamics [11–12] and micromechanics damage models (MDM) based on

* Corresponding authors.
E-mail addresses: chensian07@nudt.edu.cn (S.A. Chen), liyang16@csu.edu.cn (Y. Li).

https://doi.org/10.1016/j.compositesa.2022.107072
Received 17 February 2022; Received in revised form 6 July 2022; Accepted 8 July 2022
Available online 15 July 2022

mechanical interaction of different components [13–15]. For micromechanics damage models, the single fiber unit model is widely used in the mechanical analysis of fiber-reinforced brittle matrix composites, because it can reflect those damage mechanisms in a simplified way. For example, in the study of Rypl et al., the local equilibrium equation reflecting the functional dependence between the random variables such as mechanical properties, geometric properties and bonding properties of individual fiber and the fiber stress is derived from the single fiber unit model, which can well predict the response of composite material under uniaxial tensile load by averaging the fiber stress contributions [16]. On this basis, the elastic matrix deformations and boundary conditions restricting fiber debonding are considered in Vořechovský's model [17] and this extended single fiber model creates a link between the micromechanical formulation of a single fiber bridging action and the response of a multiply cracked composite specimen subjected to tensile loading [18].

These approaches have been able to simulate and predict strain response and limit state of composites under uniaxial loading [7,16–17]. However, due to the complex microstructure responses and interaction of CMCs during the damage process, many parameters in the existing models are hard to be determined, which increases the difficulty of performance prediction and design optimization [15–19]. Therefore, current models need to be simplified on the basis of ensuring accuracy via seizing the dominant mechanism, which has been realized in this work.

In this work, C/SiC composites were prepared via repeated impregnation of carbon fiber preforms with polycarbosilane followed by pyrolysis. The nonlinear mechanical behavior and corresponding damage mechanisms of the C/SiC composites during the cyclical loading-unloading tensile tests were investigated. Based on the damage process and its micro-mechanisms, a damage constitutive model for stiffness degradation and single fiber unit model for inelastic and elastic strain are proposed and exhibit a good correlation with the experimental results. The single fiber unit model can determine the deformation behavior according to basic macroscopic parameters such as the composition of the composite, the modulus of the fiber, matrix, and composite, the strength of the matrix and the residual thermal stress of the matrix, which is beneficial to engineering applications.

2. Materials and method

2.1. Raw materials

The reinforcement used to prepare the 2D C/SiC composites was plain carbon cloth of 1 K PAN-based carbon fibers (Toray T300B). The tensile strength and elastic modulus of the fibers are about 3000 MPa and 200 GPa, respectively. Polycarbosilane, the precursor of SiC matrix, with molecular weight ~1300 and softening point ~210 °C, was synthesized in our laboratory. The PCS/Xylene solution with a mass ratio of 1:1 was used to prepare the C/SiC composites.

2.2. Preparation of 2D-C/SiC composite

The basic preparation process of the 2D C/SiC composite is shown in

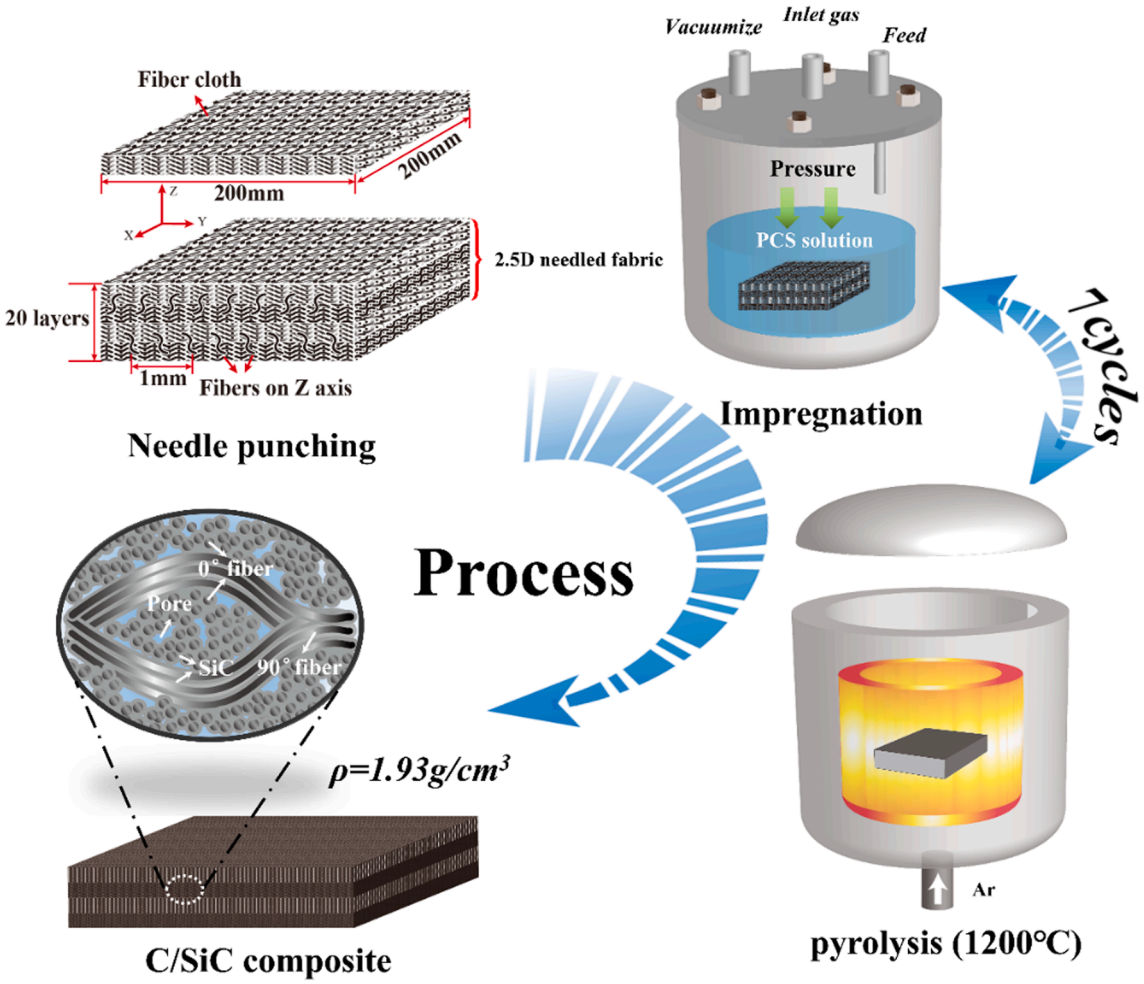

Fig. 1. Schematic diagram of preparation process of 2D-C/SiC composite. (For interpretation of the references to colour in this figure legend, the reader is referred to the web version of this article.)

Fig. 1. Firstly, the carbon fiber cloth was cut into 200 mm × 200 mm pieces, and then twenty pieces cloths were stacked and stitched in Z direction with two needles per centimeter. Finally, the preform was infiltrated in vacuum and pyrolyzed under inert gas at 1200 °C repeatedly seven times and the density of C/SiC composites increases to ~1.93 g/cm^3. The detailed preparation parameters were described in Ref. [3].

2.3. Test and characterization

In this work, all PIP C/SiC composite specimens were ground and polished. Dog-bone-shaped specimens with geometry as shown in Fig. 2 were prepared. Both monotonic tensile and cyclical loading-unloading tensile tests were performed on a servo-hydraulic testing machine Roell-Amsler System Rel 2100 manufactured by Zwick Roell Group, Ulm, Germany. The strain of specimens was measured by using an axial extensometer 632.27F-30 (MTS Systems, Eden Prairie, MN, USA) Three samples per condition were tested with a loading rate of 0.5 mm/min. The cyclic loading–unloading tests were performed with a load increment of 20 MPa per cycle up to final rupture of specimen. More details concerning the test machine and test procedure were reported in previous work [8]. The microstructure and damage morphology of the composite were characterized by scanning electron microscope (SEM, JSM-6390, JEOL, Tokyo, Japan) and back-scattered electron image (BSE).

3. Results and discussion

3.1. Microstructure and damage morphology of the C/SiC composite

Fig. 3(a) shows photographs of the C/SiC composites before and after tensile tests and the tensile direction is parallel to x-axis. The microstructure of the C/SiC composite is shown in Fig. 3(b). After the precursor infiltration pyrolysis (PIP) process, the C/SiC composite has a dense structure: silicon carbide fills most of fiber bundles and pores between fiber bundles and leaves a small number of pores in the interlayer area. Fiber bundles are mainly distributed in the horizontal (xy) plane. The 90° fiber layers are perpendicular to tensile stress and the 0° fiber layers are parallel to tensile stress. There are fewer fibers in the vertical (z) direction. The interface between carbon fibers and SiC matrix in the fiber bundles is well bonded. The larger pores between the crossing fiber bundles are also well filled with SiC matrix, showing only little residual pores. Moreover, due to the low preparation temperature and repeated impregnation cycles, possible micro-cracks caused by pyrolysis shrinkage of precursor and the mismatch of thermal expansion coefficient are less present.

Fig. 3(c-d) show the fracture morphology of the C/SiC composites observed from the vertical and horizontal directions and Fig. 3(e) shows a higher magnification of the fracture morphology of the 0° fiber layers. As shown in Fig. 3(c-d), the fracture surface of the C/SiC composite shows a stepped morphology, which is mainly caused by the different stress states and failure behaviors in the 90° and 0° fiber layers.

Different fracture morphologies of the 0° fiber layers and 90° fiber layers indicate different fracture processes and failure mechanisms. As shown in Fig. 3(c-d), the fracture morphology of 90° fiber layers consists of a large number of exposed transverse fibers, and there is no obvious fiber debonding or pull-out. Due to the direction of the applied load, the fibers in the 90° fiber layers are not effectively loaded. In this case, the fiber/matrix interface is the weak link of stress transfer due to the much lower interface bonding strength (tensile strength) in comparison to the tensile strength of the matrix and fiber. Hence, micro-cracks preferentially propagate along the fiber/matrix interface in the 90° fiber layers and converge with each other to form the fracture surface. It is worth noting that although the fiber/matrix interface tensile strength is much weaker than the tensile strength of matrix or fiber, the interface is still in a strong bonding state, causing the high efficiency of transfer load of interfacial shear stress and short pull-out length of fiber in fracture morphology (see in Fig. 3(e)).

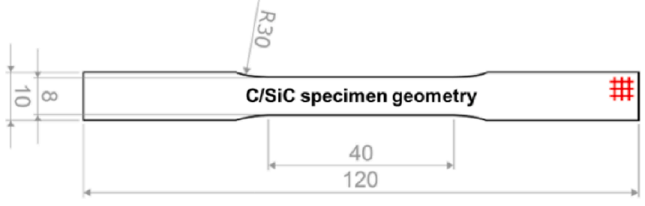

Fig. 2. Geometry of the tensile specimen. (For interpretation of the references to colour in this figure legend, the reader is referred to the web version of this article.)

As shown in Fig. 3(e), 0° fiber layers shows the phenomenon of fiber debonding and pull-out, although the pull-out length of the fiber is small. Because the fiber/matrix interface without fiber coating cannot alleviate the stress concentration through shear deformation, the stress in the end of the fibers quickly reaches the strength of the fibers, causing fracture of the fibers. As a result, the pull-out length of the fibers is short. Overall, the 0° fiber layer presents mixed fracture morphology of brittle and ductile fracture.

Obviously, crack propagation and failure occurred in 90° fiber layer prior to 0° fiber layer, showing the characteristics of stratified fracture. Moreover, as shown in Fig. 3(d), the crack preferentially propagates from the horizontal direction in the interlayer region, forming the stepped platforms between layers. This is because some pores in interlayer region are hard to be completely filled, leading to residual porosity. Due to higher stress concentration, the residual pores facilitate crack generation and propagation.

3.2. Stress–strain curve of C/SiC composites in monotonic and cyclical loading/unloading tensile tests

The tensile stress–strain curves of the specimens in the monotonic tensile test and cyclical loading/unloading tensile test are shown in Fig. 4(a) and (b), respectively. As shown in Fig. 4(a), the tensile strength and elongation of the C/SiC composite are about 215 MPa and 0.48% in the monotonic tensile test and the composite exhibits significant nonlinear behavior due to the damage evolution process. The tensile stress–strain curve can be divided into linear elastic response stage and nonlinear elastic response stage. Specifically, below the elastic limit, namely matrix cracking stress ($\sigma_{mc} = 48.8$ MPa), stress increases linearly with strain ($R^2 = 99.9\%$), whereas above the elastic limit, non-linearity with stiffness degradation is observed.

Fig. 5 shows a schematic diagram of the tensile loading–unloading stress–strain curve, illustrating the loading curve, unloading curve, elastic modulus, elastic strain (ε_e), inelastic strain (ε_p) and hysteresis loop of the composite. As shown in Fig. 4(b) and Fig. 5, every time the composite is reloaded to higher stresses, new irreversible deformation (inelastic strain) happens, and the reloading and unloading curves form a hysteresis loop during the unloading–reloading process. The width of the hysteresis loop and the new inelastic strain increases with the applied stress.

In the linear elastic response stage, due to the low load, the shear stress in the fiber/matrix interface is lower than interfacial bonding strength and cannot cause the debonding and pull-out of fibers. Because the fiber/matrix interface has not been destroyed, fibers and matrix present synergetic linear elastic deformation. Therefore, C/SiC composite shows linear-elastic behavior and constant elastic modulus in the initial stage. As shown in Fig. 4(b) however, the loading and unloading curves are still not completely overlapped in linear elastic response stage, indicating that a small extent of irreversible deformation still occurs in this stage. Due to the shrinkage during pyrolysis and thermal expansion mismatch during cooling to room temperature, there are many inherent defects such as micro-cracks and pores in the matrix.

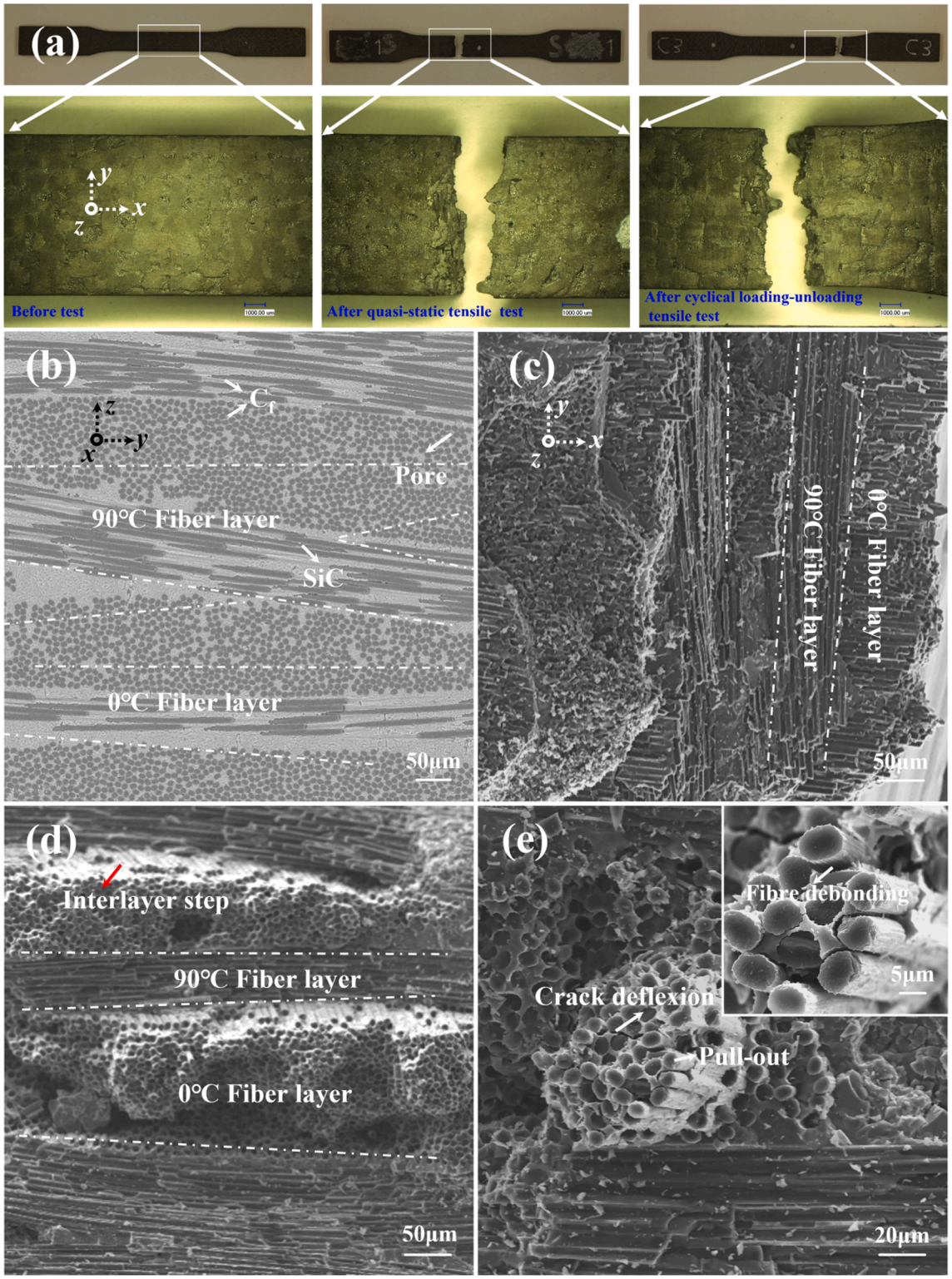

Fig. 3. (a) Photographs of the C/SiC composites before and after tensile tests; (b) microstructure of the C/SiC composite; (c-e) fracture morphology of the C/SiC composite after cyclical loading–unloading tensile test. (For interpretation of the references to colour in this figure legend, the reader is referred to the web version of this article.)

Under the action of external stress, the higher stress concentration in these defects can cause initiation and propagation cracks, leading to irreversible deformation.

As the tensile stress exceeds matrix cracking stress (48.8 MPa), the growing micro-cracks begin to coalesce and form macro-cracks in the matrix. With the cracks propagating in the matrix, the stress is more borne by the fibers. As the cracks in matrix gradually reach saturation, a series of fiber-connected matrix blocks are formed and stress is completely borne by the fibers, eventually causing the complete fracture of the composite. During this period, the gradual increase of interfacial stress causes interface debonding, sliding, pull-out and fracture of fibers. All of these damage mechanisms lead to the decrease of effective bearing

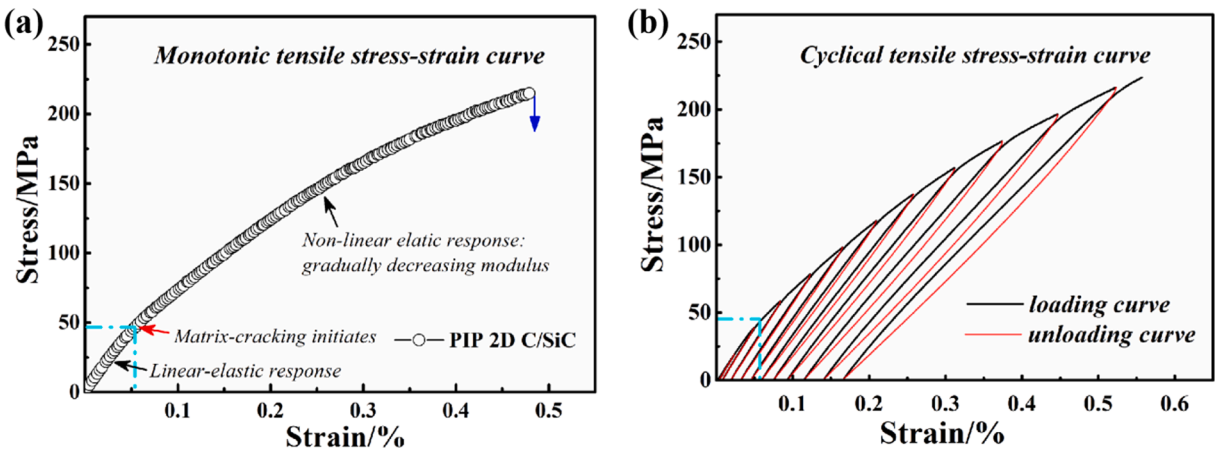

Fig. 4. (a): stress–strain curve of the composite in monotonic tensile test (b): tensile stress–strain curve of the composite in cyclical loading–unloading tensile test. (For interpretation of the references to colour in this figure legend, the reader is referred to the web version of this article.)

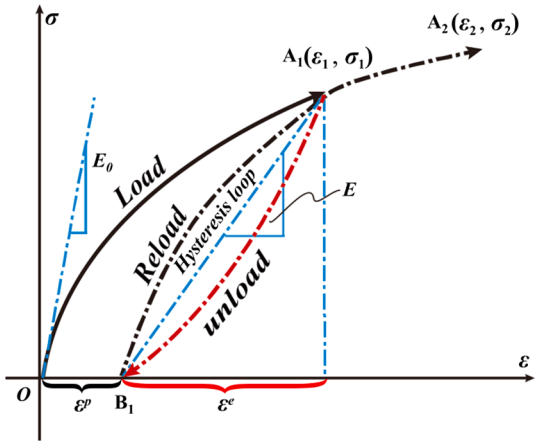

Fig. 5. Schematic diagram of the cyclical loading–unloading tensile stress–strain curve. (For interpretation of the references to colour in this figure legend, the reader is referred to the web version of this article.)

area, so the elastic modulus (E) decreases continuously, and the stress–strain curve shows nonlinear characteristics. Despite of the decrease of elastic modulus, the elastic limit (damage threshold stress) will increase, every time the composite is reloaded to the higher stress, due to the developed damage. After the composite is further damaged, the more stress is transmitted to the fiber through interface bonding and interface sliding, leading to the decrease in the load proportion of the matrix, so the further cracking of matrix needs more stress. During the loading–unloading process, unloading stress–strain curves do not coincide with the loading curves, forming irreversible deformation. Specifically, after loading process, there is more interface debonding, fiber fracture, fiber sliding than before. The interface debonding and fiber fracture cause the stress release and the fiber sliding causes the frictional resistance during deformation. Therefore, the matrix cracks are unable to heal during the unloading process. Moreover, the unloading–reloading hysteresis loop width also increases with the applied tensile strength. This is a result of the friction resistance caused by the interface sliding that delays the strain. The closed area of the hysteresis loop represents the work of the friction force. The amount of debonded fibers gradually increases with the applied stress, leading to higher friction, which results in the gradual increase of the hysteresis loop width.

In summary, damage in CMCs causes stiffness degradation and inelastic strain accumulation, which are the direct reasons for the nonlinearity of the tensile stress–strain curve of the composite. Therefore, in order to characterize the nonlinear mechanical behavior of C/SiC composites, the mechanisms of stiffness degradation and inelastic strain accumulation should be analyzed. Thus, the models for their quantitative calculation are presented below.

3.3. Damage evolution model of the C/SiC composite based on stiffness degradation

In the comparison of Fig. 4(a) and (b), it can be seen that the monotonic loading curve forms an approximate envelope of the loading–unloading curve, indicating that there is no obvious new damage in the process of unloading and reloading to the original loading point. Hence, the damage is function of the strain and applied stress. Constitutive equations of damage and strain can be constructed to characterize the damage evolution, which provides a theoretical basis for predicting the actual performance and service life of these composites under complex loads.

Based on Lemaitre's theory of CDMs that ignores the effect of hysteresis during unloading and reloading, damage value (d) is defined by the decrease of the material's stiffness [20–23]. As shown in Fig. 4(b), the linear-elastic portion remains unchanged when the stress is reloaded to the original unloading point, indicating that the elastic modulus is also dependent on the strain. Therefore, damage of the composite can be calculated by measuring the elastic modulus during the loading–unloading-reloading cycle. According to Fig. 5, the elastic modulus (E) of the damaged composite takes the slope of the connection (A_1B_1) between the unloading point (A_1) and intersection point of unloading curve and coordinate axis (B_1). The tensile damage value (d) can be defined as:

$$d = 1 - \frac{E}{E^0} \tag{1}$$

where "E" is the instant elastic modulus and "E^0," is the initial elastic modulus of the composite.

Fig. 6(a) shows the change of the modulus and corresponding damage value in relation to the strain (ε) during the cyclical loading/unloading tensile test. As shown in Fig. 6(a), with the strain increasing from 0.024% to 0.523%, the elastic modulus of the composite decreases from 95 GPa to 60 GPa and its damage value increases from 0.002 to 0.366. According to the trend of the d-ε curve, it can also be divided into three stages, corresponding to the linear elastic response stage and nonlinear elastic response stage indicating different damage mechanisms.

The damage value starts to increase near the end of the linear elastic response stage (<0.057%). During this stage, the damage development is mainly associated with matrix cracking. Prior loading, the fibers are in a compression state due to thermal stresses during processing.

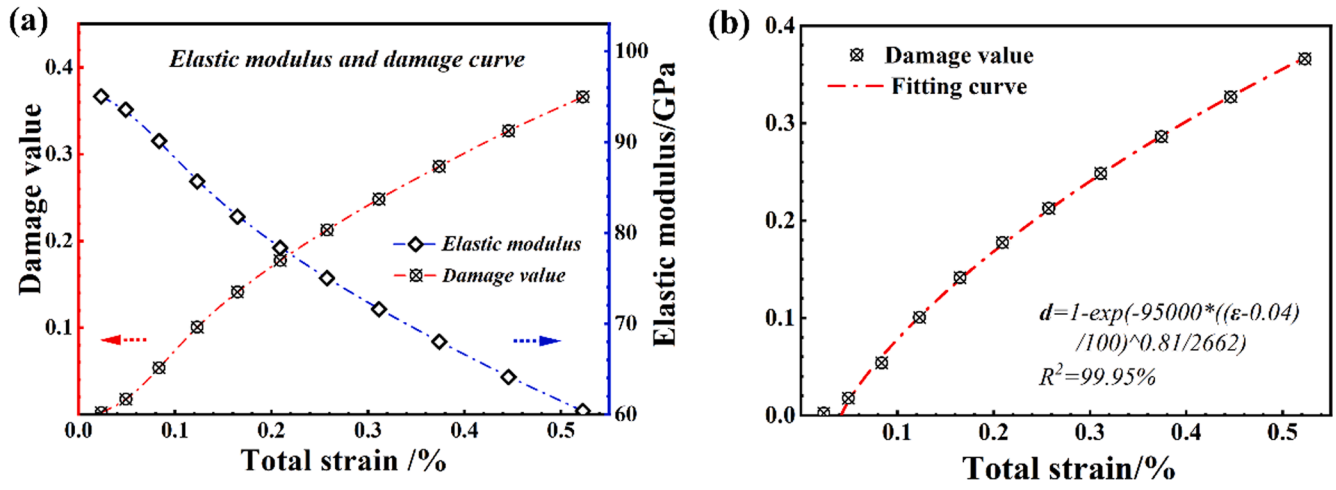

Fig. 6. The change of elastic modulus and damage value of C/SiC with strain in cyclical loading–unloading tensile test. (For interpretation of the references to colour in this figure legend, the reader is referred to the web version of this article.)

Therefore, although the damage value is lower, it accelerates to increase as the cracks propagate through the matrix, resulting in the observed concave d-ε curve in this stage.

In the nonlinear elastic response stage (0.057%-0.523%), the convex d-ε curve indicate the speed of damage accumulation gradually slows down. As the matrix cracks propagate, the fibers play a bigger role on sustaining the load. This leads to other damage mechanisms like fiber debonding, pullout and fracture. As these crack deflection mechanisms take place, part of the mechanical energy is dissipated. Therefore, the damage development rate reduces until reaching a constant value. In the latter part of this stage (0.311%-0.523%), damage value increases linearly with strain indicating constant speed of damage accumulation. The cracks in matrix have reached saturation and stress is completely borne by the fibers until the complete fracture of the composite, in accordance to previous observations.

Fracture-statistics-based approaches are appropriate for modeling the defect-induced failure of brittle materials. In this sense, the Weibull distribution provides a satisfactory approximation for damage evolution of elastic brittle material under uniaxial stress state [21–23]. In the model, the defects in composite are randomly distributed in the matrix and fiber bundles, and the fracture failure presents the feature of random brittle failure. The failure probability of a representative volume element containing fibers can be calculated as:

$$P_{\mathrm{FL}} = 1 - \exp\left\{ - \left(\frac{\sigma_{\mathrm{u}}}{\sigma_{\mathrm{w}}}\right)^{m} \right\} \tag{2}$$

where "σ_{u}" is the stress of the composite under tensile load, "σ_w" is scale parameter and "m" is Weibull modulus [23].

For the structure of woven CMCs with the number of representative volume elements of "n", it is assumed that the number of failed volume elements is "nP_{FL}", and then the number of intact volume elements is "$n(1\text{-}P_{\mathrm{FL}})$". It is assumed that elastic modulus of the representative volume element containing fibers in woven CMCs is "E_0". The load applied on the specimen is calculated as:

$$F = \sum_i \sigma_i A_0 \tag{3}$$

where "σ_i" is the stress in the volume element; "A_0" is the area of volume element.

Since the failed volume elements do not bear the load ($\sigma_i = 0$), the stress borne by the volume elements with intact fibers is

$$\sigma_i = \varepsilon E_0 \tag{4}$$

where E_0 is elastic modulus of volume element; "ε" is the elastic strain of volume element.

Therefore, the load borne by entire composite is

$$F = E_0 \varepsilon A_0 (1 - P_{FL}) n = E_0 \varepsilon A (1 - P_{FL}) \tag{5}$$

where "A" is the total bearing area of the specimen.

Therefore, the apparent stress applied to the composite is

$$\bar{\sigma} = \frac{F}{A} = E_0 \varepsilon (1 - P_{FL}) \tag{6}$$

According to Eq. (1), (2) and (6), the damage value (d) can be calculated as

$$d = 1 - \frac{E}{E_0} = 1 - \frac{\bar{\sigma}/\varepsilon}{E_0} = 1 - P_{FL} = 1 - \exp\left\{ - \left(\frac{\sigma_{\mathrm{u}}}{\sigma_w}\right)^{m} \right\}$$
$$= 1 - \exp\left\{ - \left(\frac{E^0 \varepsilon}{\sigma_w}\right)^{m} \right\} \tag{7}$$

In order to reflect the microscopic damage mechanisms of the composite (see Section 3.2), initial damage and elastic response stage without damage should be considered in the damage evolution model by introducing initial damage value d^0 and location parameter ε_{th}. The initial damage is normally related to the amount of damage caused by pyrolysis shrinkage and thermal stress mismatch during the preparation of C/SiC composite. However, due to the difficulty in measuring the initial damage in the original composites, this parameter is usually assumed as zero. Hence, the damage expression Eq. (5) can be modified as

$$d = 1 - \exp\left[- \left(\frac{E_0 \langle \varepsilon - \varepsilon_{th} \rangle}{\sigma_w}\right)^{m} \right] \tag{8}$$

where$\langle\rangle$ is the operator of Macauley brackets: if $x \geq 0$, then $\langle x \rangle = x$; "ε_{th}" is the location parameter, if the tensile strain is less than εth, the composite only has elastic deformation and do not form damage.

Because the damage evolution is determined by the strain, Eq. (8) can be applied to cyclic loading–unloading tensile process. As shown in Fig. 6(b), the "ε-d" curve obtained from the cyclic loading–unloading tensile test can be fitted well by Eq. (8), with goodness of fitting of 99.95%. This shows that the model can reflect the damage evolution law of the composites from initial state to fracture failure state. The parameter values of location parameter (ε_{th}), Weibull modulus (m), and scale parameters (σ_w) reflect the intrinsic properties of the composite and can coincide with the damage evolution process of the composite, which is analyzed below.

The location parameter (ε_{th}) of the fitting curve is around 0.04% and close to the elastic limit (0.056%) indicating that there is no failure of

volume element in elastic response stage. The location parameter (0.04%) obtained by fitting the damage-strain curve is slightly lower than the elastic limit (0.056%) obtained by stress–strain curve, due to the neglect of initial damage in the model. According to the stress–strain curve of cyclic tensile, with the increase of maximum strain and damage, the elastic limit gradually increases, which is similar to the plastic deformation of metal. The increase in elastic strain is mainly due to the stress release caused by fiber debonding. In the preparation process, the thermal expansion mismatch between fiber and matrix will lead to a certain degree of damage in C/SiC composites, so the elastic limit obtained by the fitting model that ignores initial damage is slightly lower than the actual value. The value of Weibull modulus (m) and scale parameter (σ_w), obtained by fitting the experimental data, is around 0.81 and 2662 MPa, respectively. According to the signification of Weibull distribution, the value of Weibull modulus reflects the variation trend of failure rate of volume element with strain: as the Weibull modulus (m = 0.81) is less than 1, the failure rate decreases with the increase of strain, which is consistent with the above analysis on the nonlinear elastic response stage: with the strain increasing, damage accumulation gradually slows down and tends to be constant because fibers bear more load and suppress crack propagation through debonding, fracture and pull-out. The scale parameter (2662 MPa) is an order of magnitude higher than the tensile strength of the composite material (215 MPa) because the composite will fail when reaching the damage tolerance (d^{cr} = 0.366) rather than damage saturation (d = 1). Specifically, when the damage value approaches the damage tolerance, the cracks in matrix have reached saturation and the stress is mainly borne by fibers. Further increasing the load, the inelastic strain of the composites will not occur while the rapid spread of matrix cracks and brittle fracture of the fibers lead to the failure of composite.

3.4. Single fiber unit model for the strain of C/SiC composite

The accumulation of inelastic strain with total strain and the change of inelastic strain, elastic strain and total strain with tensile stress are shown in Fig. 7(a) and (b), respectively. As shown in Fig. 7(a), inelastic strain increases linearly with strain (R2 = 100.0%), indicating that the ratio of inelastic strain and total strain is a constant (0.33). Besides, the fitting line intersects the positive half axis of the x-axis, coinciding with the previous analysis, because there is no inelastic strain at relatively lower stress (0.021%).

To describe the failure process of the composites in Section 3.2, a single fiber unit model can be constructed, as shown in Fig. 8. In the model, the diameter of the fiber is "d_f", which is coated by the matrix with a thickness of "$(D\text{-}d_f)/2$". The axial direction of the fiber is parallel to the applied tensile stress (x-axis). The elastic strain and inelastic strain of the composite can be estimated by analyzing the stress distribution in fiber, matrix and fiber/matrix interface, before and after loading and unloading.

3.4.1. Construction of single fiber unit model

Single fiber unit model is a shear-lag model of matrix crack bridging by single fiber, which can reflect the stress state and interaction between fiber and matrix in the damage process of fiber toughening brittle matrix composites. In fact, due to the heterogeneity of fiber reinforcement, the properties of fiber, matrix, and interface are random variables related to microstructure [16–18]. However, in order to simplify the analysis, the basic parameters in the composites are the average values in their statistical significance which do not affect their physical meaning and calculation process.

(1) Crack spacing in the model

In the preparation process, due to the mismatch of thermal expansion, residual tensile stress accumulates in the matrix leading to matrix transverse cracks. For the model, it is assumed that the cracks are uniformly distributed with a spacing of "L" that is the statistical average of crack spacing. A very narrow fragment (x_0, $x_0 + dx$) of the unit is taken for the analysis (see Fig. 8(b)). Assuming that the axial tensile stress $\sigma_m(x)$ at one end of the matrix ($x = x_0$) is σ_0, the corresponding tensile force is $F_1 = \pi\sigma_0(D^2 - d_f^2)/4$. The tensile force at the other end of the matrix ($x = x_0 + dx$) is $F_2 = \pi\left(\frac{\partial\sigma_m(x_0)}{\partial x}dx + \sigma_0\right)\left(D^2 - d_f^2\right)/4$. The total shear force on the fiber/matrix interface is $F_3 = \pi d_f dx\tau_m$ where "τ_m" is the shear strength of the interface. According to the force balance of the matrix ($F_2 = F_1 + F_3$), the equation can be simplified as

$$\frac{\partial\sigma_m(x)}{\partial x} = \frac{4d_f\tau_m}{D^2 - d_f^2} \tag{9}$$

Integrating both sides of Eq. (9), stress distribution function of matrix can be obtained as:

$$\sigma_m(x) - \sigma_m(x_0) = \int_{x_0}^{x_1}\frac{4d_f\tau_m}{\left(D^2 - d_f^2\right)}dx = \frac{4d_f\tau_m}{\left(D^2 - d_f^2\right)}(x - x_0) \tag{10}$$

Let x_0 and $\sigma(x_0)$ be equal to 0 ($\sigma_m(0) = 0$). When the "x" value is equal to the "L", matrix stress reaches the yield limit ($\sigma_m(L) = \sigma Ru$). According to Eq. (10), the crack spacing (L) can be calculated as:

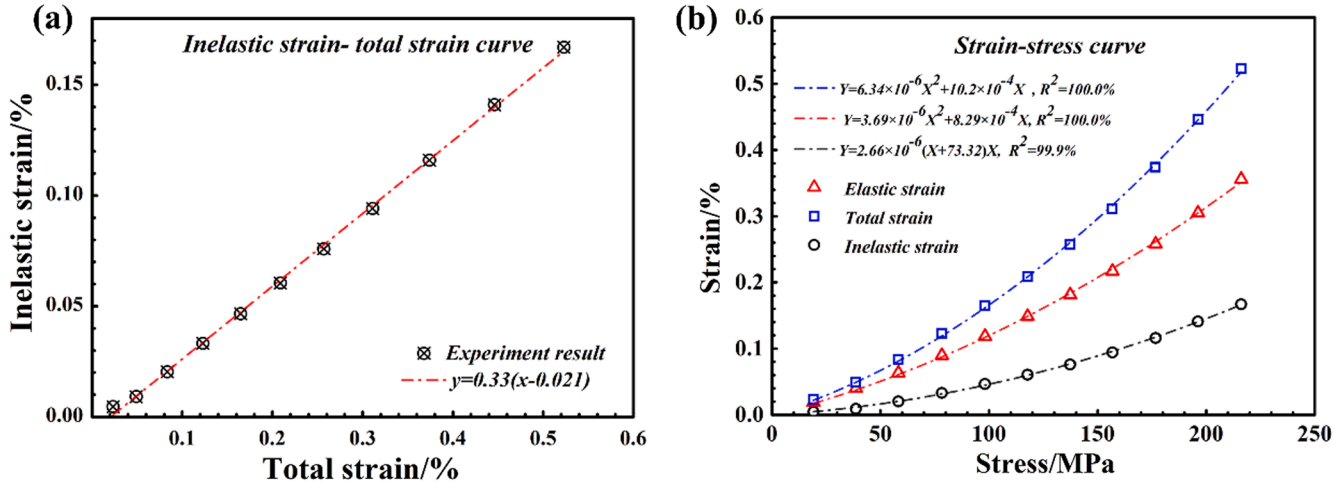

Fig. 7. (a) Change of inelastic strain with tensile strain; (b) change of inelastic strain, elastic strain and total strain with tensile stress. (For interpretation of the references to colour in this figure legend, the reader is referred to the web version of this article.)

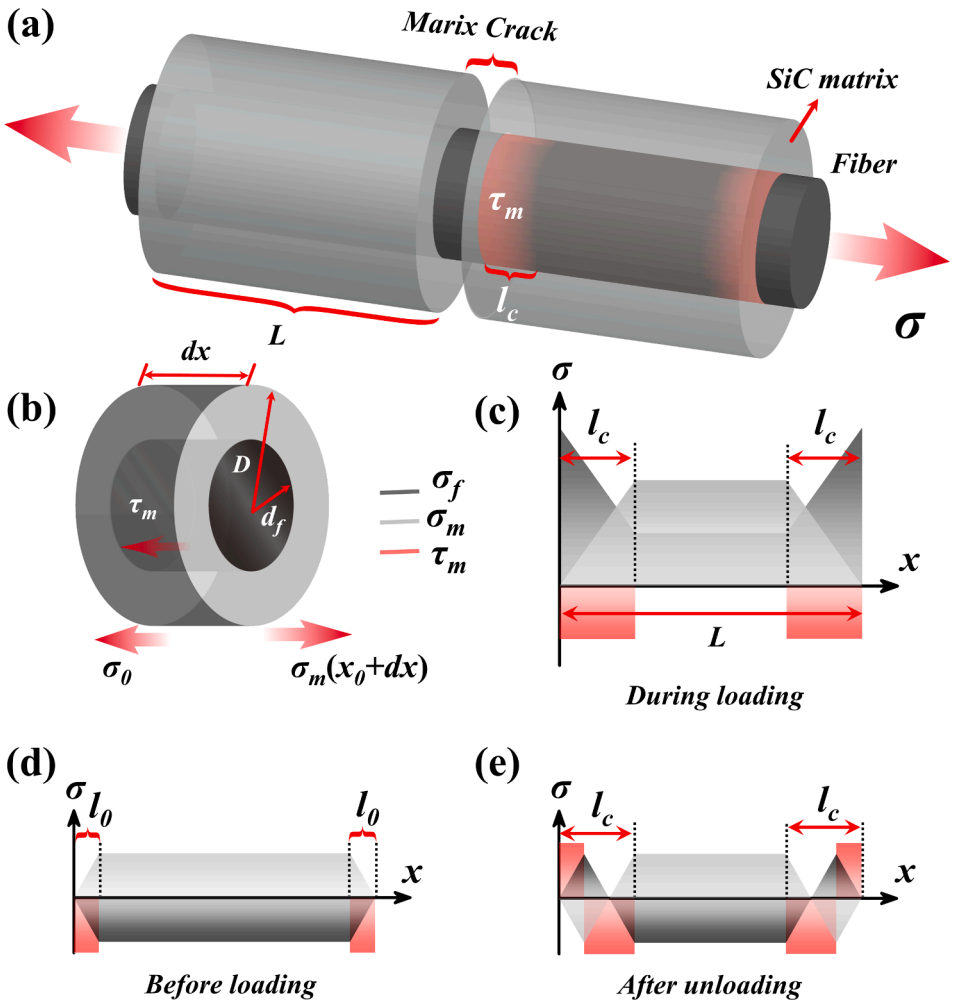

Fig. 8. Diagram of single fiber unit model: (a) single fiber unit; (b) the narrow fragment (x_0, $x_0 + dx$) of the unit; (c) the stress distribution in the unit after loading; (d) the stress distribution in the unit before loading (e) the stress distribution in the unit after unloading. (For interpretation of the references to colour in this figure legend, the reader is referred to the web version of this article.)

$$L = \frac{D^2 - d_f^2}{4d} \times \frac{\sigma_{Ru}}{\tau_m} \tag{11}$$

where "σ_{Ru}" is yield limit of the matrix.

(2) Length of the interfacial debonding region in the model

As the crack propagates, the interaction between the cracks will affect the boundary conditions limiting the fiber debonding at crack bridge boundaries, and then affect the debonding length [17]. However, in order to simplify the model and highlight the main factors, the model assumes that the matrix cracks around the infinite fiber are parallel and uniformly distributed, so the interaction between the cracks offsets each other.

When the applied tensile stress is "σ", at the matrix cracks ($x = 0$ or $x = L$), the normal stress in the matrix is zero ($\sigma_m(0) = 0$), and the applied stress is only sustained by the fibers ($\sigma_f(0) = \sigma D2/d_f^2$). Due to the strain mismatch between matrix and fiber, the interfacial shear stress reaches the interfacial shear strength (τ_m), causing interfacial debonding with the length of "l_c". According to Eq. (9) and $\sigma_m(0) = 0$, the tensile stress distribution of matrix in the debonding region ($x \in (0, l_c)$) is obtained as (see Fig. 8(c))

$$\sigma_{m'}(x) = \frac{4d_f\tau_m}{D^2 - d_f^2}x \tag{12}$$

At the boundary of the debonding region ($x = lc$), the fiber and the matrix keep synergetic elastic deformation and the elastic strain (ε) can be calculated as:

$$\varepsilon = \frac{D^2\sigma}{E_f d^2 - E_m(D^2 - d_f^2)} \tag{13}$$

where "E_f" and "E_m" are elastic modulus of fibers and matrix, respectively.

Therefore, at the boundary of the debonding region ($x = l_c$), the normal stresses in matrix and fiber are

$$\sigma_{m'}(l_c) = \frac{E_m D^2\sigma}{E_f d^2 - E_m(D^2 - d_f^2)} = \frac{E_m\sigma}{E_0} \quad E_0 = \frac{E_f d^2 - E_m(D^2 - d_f^2)}{D^2} \tag{14}$$

$$\sigma_{f'}(l_c) = \frac{E_f\sigma}{E_0} \tag{15}$$

By introducing Eq. (14) into Eq. (12), debonding length can be obtained as

$$l_c = \frac{D^2 - d_f^2}{4d} \times \frac{E_m}{E_0} \times \frac{\sigma}{\tau_m} = k\sigma; \quad k = \frac{(D^2 - d_f^2)E_m}{4dE_0\tau_m} \tag{16}$$

3.4.2. Elastic strain function compared with experimental results

(3) Stress distribution function in matrix and fibers under loading

When the interface is not completely debonded ($L > 2l_c$), the single fiber unit can be divided into the debonding region (0, l_c) and the synergistic elastic region (l_c, L-l_c). According to the force balance of the fiber, the equation of static equilibrium can be simplified as

$$\frac{\partial \sigma_{f'}(x)}{\partial x} = \frac{4\tau_m}{d_f} \quad x \in (0, l_c) \tag{17}$$

Integrating both sides of Eq. (17), the stress distribution function of fiber ($\sigma_{f'}(x)$) in the debonding region (0, l_c) can be obtained as.

$$\sigma_{f'}(\boldsymbol{x}) - \sigma_{f'}(x_0) = \int_{x_0}^{x} \frac{4\tau_m}{d_f} d\boldsymbol{x} = \frac{4\tau_m}{d_f}(\boldsymbol{x} - x_0) \quad x \in (0, l_c) \tag{18}$$

By introducing the initial condition ($\sigma_f(0) = \sigma D^2/d^2$) into Eq. (18), the stress distribution function of fiber in the debonding section can be written as (see Fig. 8(c))

$$\sigma_{f'}(\boldsymbol{x}) = \frac{\sigma D^2}{d_f^2} - \left(\frac{4\tau_m}{d_f}\right)\boldsymbol{x} \quad x \in (0, l_c) \tag{19}$$

(4) Elastic strain function under loading

According to the stress distribution function of matrix (Eq. (12)) and fiber (Eq. (19)) in the debonding region, the elastic deformation amount of fiber and matrix are calculated as:

$$\Delta l_{f'}(\boldsymbol{l}_c) = \int_0^{l_c} \frac{\sigma_{f'}(\boldsymbol{x})}{E_f} dx = \frac{\sigma D^2}{d_f^2 E_f}\boldsymbol{x} - \left(\frac{2\tau_m}{d_f E_f}\right)\boldsymbol{x}^2 \Big|_0^{l_c} = \left(\frac{D^2}{d_f^2} - \frac{2\tau_m k}{d_f}\right)\frac{k\sigma^2}{\lambda E_f} \tag{20}$$

$$\Delta l_{m'}(\boldsymbol{l}_c) = \int_0^{l_c} \frac{\sigma_{m'}(\boldsymbol{x})}{E_m} dx = \frac{2d\tau_m}{(D^2 - d_f^2)\lambda E_m}\boldsymbol{x}^2 \Big|_0^{l_c} = \frac{2d\tau_m}{(D^2 - d_f^2)\lambda E_m}k^2\sigma^2 \tag{21}$$

The stress of fiber and matrix in the synergistic elastic region are equal to that at the boundary of the debonding region, so according to Eq. (14) and (15), the elastic deformation of fiber and matrix in the synergistic elastic region (l_c, L-l_c) is calculated as:

$$\Delta l_{f''} = \Delta l_{m''} = \int_{l_c}^{L-l_c} \frac{\sigma}{E} dx = \frac{\sigma}{E_0}(L - 2k\sigma) \tag{22}$$

In the single fiber unit, the elastic strain of the fiber represents the total elastic strain of the unit because the fiber maintains an elastic continuum. However, due to the existence of transverse fibers (parallel to y-axis direction) and pores, the actual modulus of the composite should be "λE_0" where "λ" is the apparent coefficient, and the corresponding apparent modulus of the fiber and the matrix are "λE_f" and "λE_m", respectively. Therefore, the elastic strain function of the composite is

$$\varepsilon_e(\sigma) = \Delta l_e \Big/ L = \left(2\Delta l_{f'}(l_c) + \Delta l_{f''}\right) \Big/ L = \frac{1}{\lambda E_0}\sigma + \frac{E_m^2}{E_0^2 E_f \lambda} \times \frac{D^2 - d_f^2}{d_f^2} \times \frac{\sigma^2}{\sigma_{Ru}} \tag{23}$$

(5) Comparison of elastic strain function with experimental results

Fig. 7(b) shows the elastic strain–stress curve fitted by the elastic strain function. It can be found that the elastic strain function can fit the elastic strain–stress curve well ($R^2 = 100.0\%$) and the coefficients of the quadratic term and the first term in the function are 3.689×10^{-8} MPa^{-2} and 8.292×10^{-6} MPa^{-1}, respectively. The elastic modulus of T300 fibers and SiC matrix is about 200 GPa and 400 GPa, respectively [22]. According to the density of the fiber preform ($\rho = 0.75$ g/cm^3), the volume fraction of fibers is 42%. According to the weight gain of composites during PIP process and the density of pyrolysis products of polycarbosilane ($\rho = 2.7$ g/cm^3), the volume fraction of SiC matrix is around 44 % and the residual porosity is about 14%. The diameter of fiber (d_f) is 7 μm. According to the volume ratio of fiber and matrix, the diameter of single fiber unit (D) is about 10 μm. Based on Eq. (15), the modulus of single fiber unit in synergistic elastic region can be calculated as E_0 = 302.3 GPa.

A large number of studies have shown that the elastic modulus of dense C/SiC composites is in the range of 90–130 GPa [4–5,9,11]. According to Eq. (23), the actual modulus of the undamaged C/SiC composite should be 120.6 GPa with the apparent coefficient of 0.4, which falls within the usual elastic modulus range of C/SiC composites. Substituting $E_f = 2 \times 10^5$ MPa, $E_m = 4 \times 10^5$ MPa, $E0 = 3.01 \times 10^5$ MPa, $\lambda = 0.4$, $D = 10$ μm and d = 7 μm into the quadratic term of elastic strain function ($\varepsilon_e(\sigma)$), the yield strength of SiC matrix can be obtained as σ_{Ru} = 631 MPa. According to C. Chateau's study, the strength of SiC is around 600–700 MPa proving the single fiber unit model is reasonable for C/SiC composites without interface phase [15].

According to the Eq. (2) and (3), only when the applied tensile stress reaches 299 MPa, the fiber will be completely debonded ($2l_c = L$). Since the strength of the composite is only 216 MPa, the composite fails before the complete debonding of the fibers ($l_c < L/2$). This can be seen in the fracture morphology of Fig. 2 (d). Therefore, the model does not need to consider the different stress distribution function after the interface is completely debonded (L-$2l_c < 0$).

3.4.3. Inelastic strain function compared with experimental results

Using the model, the inelastic deformation after unloading can be determined by the stress distribution before loading and after unloading, which is analyzed as follows. The mismatch of thermal expansion coefficient between fiber and matrix results in the internal stress in the preparation process, which determines the stress distribution in the composite before loading. When the composite is cooled from the preparation temperature to room temperature, the fibers and the matrix show different degrees of shrinkage ($\alpha_m \Delta T > \alpha_f \Delta T$) due to the different thermal expansion coefficient ($\alpha_m > \alpha_f$). However, due to the mutual constraint of the fiber and the matrix through the interface, the fiber and matrix actually have the same degree of deformation (e), that is the synergistic elastic deformation ($\alpha_m \Delta T > e > \alpha_f$).

Due to the mutual constraint, the compressive stress in the fibers is:

$$F_f = \frac{\pi}{4} d_f^2 (e - \alpha_f \Delta T) E_f \tag{24}$$

The tensile stress in the matrix is

$$F_m = \frac{\pi}{4}\left(D^2 - d_f^2\right)(\alpha_m \Delta T - e) E_m \tag{25}$$

Since "F_f" and "F_m" are mutual reaction forces ($F_f = F_m$), the strain of the single fiber unit (e) can be calculated as:

$$e = \frac{\alpha_f E_f d_f^2 + \alpha_m E_m \left(D^2 - d_f^2\right)\Delta T}{E_0 D^2} \tag{26}$$

(6) Stress distribution function in matrix and fibers before loading

By combining Eq. (26) and Eq. (25), the tensile stress in the matrix can be calculated as:

$$\sigma_m = \left(\alpha_m - \frac{\alpha_f E_f d_f^2 + \alpha_m E_m \left(D^2 - d_f^2\right)}{E_0 D^2}\right) E_m \Delta T \tag{27}$$

When the composite is cooled to a certain temperature, that is the matrix cracking temperature (T_{mc}), the tensile stress in the matrix (σ_m) exceeds the yield strength (σ_{Ru}) of the matrix, causing transverse microcracks and release of thermal stress. Therefore, the value of "T_{mc}" can be calculated as

$$T_{mc} = T_p - \frac{E_0 D^2 \sigma_{Ru}}{E_m E_f d_f^2 (\alpha_m - \alpha_f)} \tag{28}$$

According to existing reports, the average thermal expansion coefficient (α_m) of SiC at 0-1200℃ is around 5.93 × 10^{-6}/K [20–21], and by comparison the axial thermal expansion coefficient of carbon fiber can be neglected. Therefore, considering the values of "E_f", "E_m", "E_0", "σ_{Ru}", "D", "d_f", and "α_m" for the composite, the matrix cracking temperature (T_{mc}) is calculated as around 373℃. In fact, due to the stress concentration caused by the inherent defects, micro-cracks will occur when the temperature is much higher than 373 °C. However, with the temperature dropping below 373 ℃, the transverse micro-cracks at the interface will reach saturation and be distributed uniformly with the crack spacing of "L". It can be considered that, at matrix cracking temperature, most of the thermal stress can be released by the formation of micro-cracks. With the temperature further decreasing, the number of cracks will not increase, and the matrix will only release the stress through the growth of micro-cracks and interface debonding. Therefore, after the composite is cooled to room temperature, a certain degree of residual tensile thermal stress (σ_{pre}) will still be accumulated in the matrix. Therefore, the stress distribution function in matrix and fibers before loading are obtained as (see Fig. 8(d))

$$\sigma_m(x)=\begin{cases}\dfrac{4d_f\tau_m}{D^2-d_f^2}x & \left(0<x<l_0, l_0=\dfrac{\left(D^2-d_f^2\right)\sigma_{pre}}{4\tau_m d_f}\right)\\ \sigma_{pre} & (l_0<x<L-l_0)\\ \dfrac{4d_f\tau_m}{D^2-d_f^2}(L-x) & (L-l_0<x<l_0)\end{cases} \tag{29}$$

$$\sigma_f(x)=\begin{cases}\dfrac{4\tau_m}{d_f}x & \left(0<x<l_0, l_0=\dfrac{D^2-d_f^2\sigma_{pre}}{4\tau_m d_f}\right)\\ \dfrac{\left(D^2-d_f^2\right)\sigma_{pre}}{d_f^2} & (l_0<x<L-l_0)\\ \dfrac{4\tau_m}{d_f}(L-x) & (L-l_0<x<l_0)\end{cases} \tag{30}$$

(7) Stress distribution function in matrix and fibers after loading

Due to the undamaged interface, the synergistic elastic region ($l_c < x < L\text{-}l_c$) can be restored to the original state ($\sigma_f = \sigma_{pre}(D^2\text{-}d^2)/d^2$, $\sigma_m = \sigma_{pre}$) after unloading and shows no irreversible deformation. The stress at both ends of the debonding region ($x = 0$ and $x = l_c$) can be determined as:

$$\begin{cases}\sigma_f(0)=\sigma_m(0)=0\\ \sigma_m(l_c)=\sigma_{pre}\\ \sigma_f(l_c)=\sigma_{pre}(D^2-d^2)/d^2\end{cases} \tag{31}$$

Theoretically, if there is no shear interaction between the fiber and matrix in the debonding region, then after the external stress is removed, the fiber and matrix would recover to their original state. The extended fiber segments would shrink back to the matrix, causing the micro-cracks to heal. In fact the shear strength of the fiber/matrix interface in the debonding section of the model is "τ_m" as previously mentioned. Because the two ends of the debonding region ($x = 0$ and $x = l_c$) are considered as free ends and the fiber has much lower elastic modulus than the SiC matrix, both fiber and matrix of the debonding region shrink in the direction from the ends to the center during unloading. However, the strain of the fiber is larger than that of the matrix, causing interface shear stress. Therefore, the stress distribution functions of fiber and matrix in the debonding section are (see Fig. 8(e)):

$$\sigma_m(x)=\begin{cases}-\dfrac{4d_f\tau_m}{D^2-d_f^2}x & \left(0<x<l_c\Big/2-\dfrac{\left(D^2-d_f^2\right)\sigma_{pre}}{8\tau_m d_f}l_0\right)\\ \dfrac{4d_f\tau_m}{D^2-d_f^2}(x-l_c)+\sigma_{pre} & \left(l_c\Big/2-\dfrac{\left(D^2-d_f^2\right)\sigma_{pre}}{8\tau_m d_f}l_0<x<l_c\right)\end{cases} \tag{32}$$

$$\sigma_f(\boldsymbol{x})=\begin{cases}\dfrac{4\tau_m}{d_f}\boldsymbol{x} & \left(0<\boldsymbol{x}<l_c\Big/2-\dfrac{(D^2-d_f^2)\sigma_{pre}}{8\tau_m d_f}l_0\right)\\ \dfrac{4\tau_m}{d_f}(l_c-\boldsymbol{x})+\dfrac{(D^2-d_f^2)\sigma_{pre}}{d_f^2} & \left(l_c\Big/2-\dfrac{(D^2-d_f^2)\sigma_{pre}}{8\tau_m d_f}l_0<\boldsymbol{x}<l_c\right)\end{cases} \tag{33}$$

(8) Inelastic strain function in the model

According to the difference between the stress distributions before loading Eq. (29)–(30) and after unloading Eq. (32)–(33), the deformation amount of the fiber and matrix in the debonding section are:

$$\Delta l_f(l_c)=\frac{\tau_m}{\mathrm{d}_f\lambda E_f}k^2\left(\sigma+\frac{E_m}{E_0}\sigma_{pre}\right)\sigma \tag{34}$$

$$\Delta l_{\mathrm{m}}(l_c)=-\frac{\tau_m d}{(D^2-d_f^2)\lambda E_m}k^2(\sigma+\frac{E_m}{E_0}\sigma_{pre})\sigma \tag{35}$$

The relative displacement between the fiber and matrix is the crack width of the matrix, namely the irreversible deformation of the composite after unloading. Since there is no irreversible deformation in the synergistic elastic region, the total irreversible deformation is equal to the difference between the deformation amount of fiber and matrix in in the debonding section:

$$\Delta l_p=2\times(\Delta l_f(l_c)-\Delta l_{\mathrm{m}}(l_c))=\frac{2E_0D^2k^2\tau_m(\sigma+\frac{E_m}{E_0}\sigma_{pre})\sigma}{\lambda E_m E_f(D^2-d_f^2)d_f} \tag{36}$$

Therefore, the inelastic strain of the composite is

$$\varepsilon_p=\Delta l_p\Big/L=\frac{E_m}{\lambda E_f E_0}\times\frac{D^2}{2d_f^2}\times\frac{\left(\sigma+\dfrac{E_m}{E_0}\sigma_{pre}\right)\sigma}{\sigma_{Ru}}=\alpha(\sigma+\sigma_{pre}^{'})\sigma$$
$$\alpha=\frac{E_mD^2}{2\lambda E_f E_0 d_f^2\sigma_{Ru}}\quad\sigma_{pre}^{'}=\frac{E_m}{E_0}\sigma_{pre} \tag{37}$$

(9) Comparison of inelastic strain function with experimental results

As shown in the Fig. 7(b), the inelastic strain function Eq. (37) can accurately fit the inelastic strain–stress curve with R^2 of 99.9% and the value of "α" and "σ_{pre}" are obtained as 2.66 × 10^{-8} MPa^{-2} and 54.99 MPa. By Substituting $E_f = 2 \times 10^5$ MPa, $E_m = 4 \times 10^5$ MPa, $E_0 = 3.01 \times 10^5$ MPa, $\lambda = 0.4$, $D = 10$ μm, $d = 7$ μm, and $\sigma_{Ru} = 631$ MPa into the expression of "α", the value of "α" is equal to 2.70 × 10^{-8} MPa^{-2}, which is very close to the "α" value obtained by the fitting curve (2.66 × 10^{-8} MPa^{-2}), proving the reliability of the single fiber unit model for the C/SiC composite.

In Broda's study, the residual stress state of C/SiC composites was analyzed by X-ray diffraction [22]. A relation between the bonding strength and the residual thermal stresses in C/SiC was observed. After cooling down, the residual stress of C/SiC composites with pitch coated fibers (ca. 50 MPa) that have stronger interface bonding is much lower than that of C/SiC composite with pyrolytic carbon (PyC) coated fiber (ca. 110 MPa). In general, strong interface bonding causes more release of thermal load by further crack formation during the cooling down of the composite. The residual stress in matrix (σ_{pre}) obtained by fitting the

inelastic strain–stress curve is equal to 54.99 MPa that is close to that of the C/SiC composites with pitch coated fibers in M. Broda's study. This is in good accordance with our study since the C/SiC composites in our study have no fiber coating, meaning a relatively strong interface bonding. According Eq. (23) and (36), compared with fiber, the higher volume content and modulus of the matrix mean the lower the ratio of inelastic deformation and elastic deformation, which can be proved by the comparison with the C/SiC composite prepared by CVI. The C/SiC composites in Wang and Mei studies have the same carbon fiber type (Toray T300), similar fiber content (40%, 40 ± 2%) and matrix content to our study, but the ratio of inelastic deformation to elastic deformation is significantly lower (0.34, 0.38) than that in our study (0.5) [4,14]. Because the SiC matrix in their C/SiC composites are prepared by CVI rather than PIP process and CVI-SiC has the much higher density and elastic modulus than that of PIP-SiC, causing the lower ratio.

In summary, this model considers the influence of fiber debonding, interface sliding and matrix cracking on stress and strain and has a good fitting effect on the mechanical properties of the C/SiC composites without interface phase, reflecting the damage and failure mechanism of composites.

4. Conclusions

In this study, the nonlinear mechanical behavior and damage mechanisms of C/SiC composites prepared by PIP process were investigated. Based on the damage mechanisms, models for stiffness degradation and elastic and inelastic deformation were proposed. The main results are as follows:

(1) The fracture surface of the C/SiC composite shows a stepped morphology with interlayer fracture, which is mainly caused by the different stress states and failure behaviors in the 90° and 0° fiber layers. In 90° fiber layers, the interfaces are the weak link of stress transfer causing premature failure, whereas 0° fiber layers present a mixed morphology of brittle and ductile fracture with fiber debonding, pull-out and fracture.

(2) Damage mechanics in composite such as matrix cracking, interfacial debonding and sliding, and fiber fracture causes stiffness degradation, inelastic strain accumulation, and hysteresis loop, which are the direct reasons for the nonlinearity response as the stress exceeds matrix cracking stress. Due to the different damage mechanisms, the linear elastic response and nonlinear elastic response stages present different damage evolution trends which can be fitted by Weibull failure probability (Eq. (8)).

(3) According to the damage mechanisms including matrix cracking, interfacial debonding and sliding, a single fiber unit model was established to obtain the elastic and inelastic deformation law of the composite. In the model, based on stress distribution during processing (Eqs. (10, 27, 29–30)), loading (Eqs. (12, 14, 15, 19)) and unloading (Eqs. (32–33)), elastic and inelastic strain formulas (Eqs. (23, 36)) for the composites were proposed. These can perfectly fit the experimental results ($R^2 > 99.9\%$). The model demonstrates the relation between deformation law of the composite and the basic macroscopic parameters such as the composition of the composite, the elastic modulus of the fiber, matrix, and composite, the strength of the matrix and the residual thermal stress of the matrix in a simple way.

CRediT authorship contribution statement

Z.B. Niu: Validation, Formal analysis, Investigation, Data curation, Writing – original draft, Visualization. **S.A. Chen:** Conceptualization, Methodology, Resources, Writing – review & editing. **Y. Li:** Conceptualization, Methodology, Validation, Formal analysis, Data curation, Writing – review & editing, Supervision, Project administration, Funding acquisition. **P. Xiao:** Validation, Data curation. **Z.M. Yang:** Methodology, Resources, Data curation, Investigation. **Y.G. Tong:** Methodology, Resources, Data curation. **R.S.M. Almeida:** Validation, Investigation, Data curation, Writing – review & editing.

Declaration of Competing Interest

The authors declare that they have no known competing financial interests or personal relationships that could have appeared to influence the work reported in this paper.

Data availability

Data will be made available on request.

Acknowledgements

The authors gratefully acknowledge the financial supports from National Natural Science Foundation of China (Grant No. 52102122 and 52173306) and National Key Laboratory of Science and Technology on High-strength Structural Materials, Central South University (Grant No. SYSJJ2021LWS01).

Appendix

symbol	physical quantity	symbol	physical quantity
σ_{mc}	matrix cracking stress	ε_e	elastic strain
ε_p	inelastic strain	L	crack spacing
E^0	initial elastic module	d	damage value
ε_{th}	location parameter	σ_w	scale parameter
m	shape parameter	D	diameter of the single fiber unit
d_f	diameter of the fiber	σ_{Ru}	yield limit of matrix
E_f	elastic modulus of fibers	E_m	elastic modulus of matrix
E_0	elastic modulus of the unit	τ_m	shear strength of the interface
σ_f	tensile stress of fiber	σ_m	axial tensile stress of matrix
l_p	debonding length	Δl_e	elastic deformation
Δl_e	irreversible deformation	λ	apparent coefficient of elastic modulus
T_{mc}	matrix cracking temperature	σ_{pre}	residual tensile thermal stress

References

[1] Tang Z, Yi M, Zhou Y, Liu R, Peng Ke. Effect of high-temperature heat treatment on the microstructure and mechanical behavior of PIP-based C/C-SiC composites with SiC filler. J Eur Ceramic Soc 2021;41(15):7610–9.

[2] Li Y, Xiao P, Luo H, Almeida RSM, Li Z, Zhou W, et al. Fatigue behavior and residual strength evolution of 2.5D C/C-SiC composites. J Eur Ceram Soc 2016;36 (16):3977–85.

[3] Dang X, Zhao D, Guo T, et al. **Oxidation behaviors of carbon fiber reinforced multilayer SiC-Si_3N_4 matrix composites**. J Adv Ceram 2022;11(2):365–77. https://doi.org/10.1007/s40145-021-0540-8.

[4] Hui M. Measurement and calculation of thermal residual stress in fiber reinforced ceramic matrix composites. Compos Sci Technol 2008;68(15–16):3285–92. https://doi.org/10.1016/j.compscitech.2008.08.015.

[5] Camus G, Guillaumat L, Baste S. Development of damage in a 2D woven C/SiC composite under mechanical loading: I. Mechanical characterization. Compos Sci Technol 1996;56(12):1363–72. https://doi.org/10.1016/S0266-3538(96)00094-2.

[6] Naslain R. Materials design and processing of high temperature ceramic matrix composites: state of the art and future trends. Adv Compos Mater 1999;8(1):3–16. https://doi.org/10.1163/156855199X00029.

[7] Aubard X. New advances in damage mechanics and computational methods for composites: from research to industry for spatial applications. Compos Sci Technol 2001;61(15):2337–44. https://doi.org/10.1016/S0266-3538(01)00126-9.

[8] Almeida RSM, Li Y, Besser B, Xiao P, Zhou W, Brückner A, et al. Damage analysis of 2.5D C/C-SiC composites subjected to fatigue loadings. J Eur Ceram Soc 2019;39 (7):2244–50.

[9] Beyerle DS, Spearing SM, Evans AG. Damage Mechanisms and the Mechanical Properties of a Laminated 0/90 Ceramic/Matrix Composite. J Am Ceram Soc 2010; 75(12):3321–30. https://doi.org/10.1111/j.1151-2916.1992.tb04428.x.

[10] Rensen BF, Talreja R, Rensen OT. Micromechanical analysis of damage mechanisms in ceramic-matrix composites during mechanical and thermal cycling. Composites 1993;24(2):129–40. https://doi.org/10.1016/0010-4361(93)90009-W.

[11] Xie J, Fang G, Chen Z, Liang J. An anisotropic elastoplastic damage constitutive model for 3D needled C/C-SiC composites. Compos Struct 2017;176:164–77.

[12] Chaboche JL, Maire JF. New progress in micromechanics-based CDM models and their application to CMCs. Compos Sci Technol 2001;61(15):2239–46. https://doi.org/10.1016/S0266-3538(01)00118-X.

[13] He MY, Wu B-X, Evans AG, Hutchinson JW. Inelastic strains due to matrix cracking in unidirectional fiber-reinforced composites. Mech Mater 1994;18(3):213–29.

[14] Wang Y, Zhang L, Cheng L, Mei H, Ma J. Characterization of tensile behavior of a two-dimensional woven carbon/silicon carbide composite fabricated by chemical vapor infiltration. Mater Sci Eng, A 2008;497(1-2):295–300.

[15] Chateau C, Gélébart L, Bornert M, Crépin J, Caldemaison D, Sauder C. Modeling of damage in unidirectional ceramic matrix composites and multi-scale experimental validation on third generation SiC/SiC minicomposites. J Mech Phys Solids 2014; 63:298–319.

[16] Rypl R, Chudoba R, Scholzen A, Vořechovský M. Brittle matrix composites with heterogeneous reinforcement: Multi-scale model of a crack bridge with rigid matrix. Compos Sci Technol 2013;89:98–109. https://doi.org/10.1016/j.compscitech.

[17] Vořechovský M, Rypl R, Chudoba R. Probabilistic crack bridge model reflecting random bond properties and elastic matrix deformation. Compos Part B-Eng 2018; 139:130–45.

[18] Vořechovský M, Li Y, Rypl R, et al. Tensile behavior of carbon textile concrete composite captured using a probabilistic multiscale multiple cracking model. Compos Struct 2021;277:114624. https://doi.org/10.1016/j.compstruct.2021.

[19] Kumar R. Analysis of coupled ply damage and delamination failure processes in ceramic matrix composites. Acta Mater 2013;61(10):3535–48. https://doi.org/10.1016/j.actamat.2013.02.027.

[20] Sun Z, Shan Z, Shao T, Li J, Wu X. A multiscale modeling for predicting the thermal expansion behaviors of 3D C/SiC composites considering porosity and fiber volume fraction. Ceram Int 2021;47(6):7925–36.

[21] Buet E, Sauder C, Sornin D, Poissonnet S, Rouzaud J-N, Vix-Guterl C. Influence of surface fibre properties and textural organization of a pyrocarbon interphase on the interfacial shear stress of SiC/SiC minicomposites reinforced with Hi-Nicalon S and Tyranno SA3 fibres. J Eur Ceram Soc 2014;34(2):179–88.

[22] Broda M, Pyzalla A, Reimers W. X-ray Analysis of Residual Stresses in C/SiC Composites. Appl Compos Mater 1999;6(1):51–66. https://doi.org/10.1023/A:1008885319105.

[23] Z. Yang, H. Liu, J. Yang. **Damage constitutive model for thermal shocked-ceramic matrix composite**. Chinese Journal of Theoretical and Applied Mechanics 2019;51 (6):1797-1809. doi: 10.6052/0459-1879-19-229.